

## Article

# Assessment of the Impacts of Urbanization on Landslide Susceptibility in Hakha City, a Mountainous Region of Western Myanmar

Kyaw Swar Myint Thein <sup>1,\*</sup>, Masahiko Nagai <sup>2</sup>, Tai Nakamura <sup>3</sup>, Noppadol Phienwej <sup>1</sup> and Indrajit Pal <sup>1</sup>

<sup>1</sup> Asian Institute of Technology, Pathum Thani 12120, Thailand; noppadol@ait.ac.th (N.P.); indrajit-pal@ait.asia (I.P.)

<sup>2</sup> Center for Research and Application for Satellite Remote Sensing, Graduate School of Sciences and Technology for Innovation, Yamaguchi University, Yamaguchi 753-0841, Japan; nagaim@ait.ac.th

<sup>3</sup> Japan Aerospace Exploration Agency, Tsukuba-shi 305-8505, Japan; nakamuratai@ait.ac.th

\* Correspondence: st116417@ait.asia; Tel.: +66-811-154-569

**Abstract:** In July 2015, more than 100 landslides caused by Cyclone Komen resulted in damage to approximately 1000 buildings in the mountainous region of Hakha City, Myanmar. This study aimed to identify potential landslide susceptibility for newly developed resettlement areas in Hakha City before and after urbanization. The study evaluated landslide susceptibility through statistical modeling and compared the level of susceptibility before and after urbanization in the region. The information value model was used to predict landslide susceptibility before and after urbanization, using 10 parameter maps as independent variables and 1 landslide inventory map as the dependent variable. Four landslide types were identified in the study area: shallow earth slide, deep slide, earth slump, and debris flow. Susceptibility analyses were conducted separately for each type to better recognize the different aspects of landslide susceptibility in planned urban areas. By comparing the results of the susceptibility index before and after urbanization, suitable urban areas with lower landslide susceptibility could be identified. The results showed that high-potential landslide susceptibility increased by 10%, 16%, and 5% after urbanization compared with before urbanization in three Town Plans, respectively. Therefore, Town Plan 3 is selected as the most suitable location for the resettlement area in terms of low risk of landslides.

**Keywords:** landslide inventory; landslide susceptibility; statistical modeling; information value; urban planning; resettlement



**Citation:** Thein, K.S.M.; Nagai, M.; Nakamura, T.; Phienwej, N.; Pal, I. Assessment of the Impacts of Urbanization on Landslide Susceptibility in Hakha City, a Mountainous Region of Western Myanmar. *Land* **2023**, *12*, 1036. <https://doi.org/10.3390/land12051036>

Academic Editor: Domenico Calcaterra

Received: 18 April 2023

Revised: 2 May 2023

Accepted: 3 May 2023

Published: 9 May 2023



**Copyright:** © 2023 by the authors. Licensee MDPI, Basel, Switzerland. This article is an open access article distributed under the terms and conditions of the Creative Commons Attribution (CC BY) license (<https://creativecommons.org/licenses/by/4.0/>).

## 1. Introduction

The study of landslides is complicated as it involves a variety of factors, including environmental and physical factors, as well as those driven by human interaction [1]. Spatial technologies such as remote sensing and geographic information systems (GIS) are powerful tools for predicting landslide hazards and risks on both regional and local scales. Remote sensing can be used for exploring thematic data layers such as geological features, land cover, land use, previous landslide information, and topography, while GIS plays a crucial role in analyzing the distribution of hazards, their magnitude and frequency, the impact on human property, and the loss of life and property. Additionally, GIS can be used to predict potential hazards and risks through statistical and deterministic multi-criteria modeling [2–4].

Hakha City, the capital of Chin State in western Myanmar, is susceptible to landslides due to its location in the Indo-Burma Ranges, with high relief mountains and weak rock formations [5]. The area is composed of flysch sediments with steep slope gradients ranging from 15 to 60° and is 1800 m above sea level, with its highest peak at 2299 m.

The climate in the region is cool and dry from November to February, followed by a hot summer season from February to May, and a hot, rainy season from June to October. The average total annual rainfall is 2190 mm. In July and August of 2015, Cyclone Komen caused heavy rain across Chin State [6]. On 27 July and 31 July 2015, the highest daily rainfall amounts in 25 years were recorded, measuring 182 mm and 181 mm, respectively. Nine townships in Chin State were affected by landslides. As a result, a total of 10,383 houses, 6039 farms, 303 bridges, 121 public buildings, and 2 small dams were destroyed, and 5 people were killed statewide [7]. In Hakha Township, a total of 112 landslides occurred, covering 3.63 km<sup>2</sup>, and 991 houses, 11 public buildings, and 2 bridges were destroyed, and there were no casualties [8]. As a result, a total of 732 houses were relocated to a newly developed urban area; furthermore, the Chin State Government reported a total loss of 28 billion kyats (~23 million USD) [9].

Currently, a master resettlement plan for Hakha City is being prepared by the Chin State Government. Rapid assessment was needed to relocate the 884 families living in temporary camps to a safer place by the end of October 2015 [10]. Typically, this type of urban planning involves multiple tasks such as considering housing, resource availability, land use, transportation, and the environment. With the increasing impact of climate change and natural disasters, disaster risk reduction and resilience planning have become critical components of urban planning. This study used GIS and spatial modeling to assess the changes in hazard levels before and after urbanization in a planned area. Although Hakha City is a landslide-prone area, there are currently no existing data on landslide occurrences in the area. This study presents the first landslide susceptibility assessment for the region. The findings from this study can be used to formulate essential hazard mitigation plans and to determine the efficacy of target resettlement areas.

Landslide susceptibility mapping can be carried out by three methods: heuristic, deterministic, or probabilistic statistical methods. In the heuristic method, the landslide susceptibility map is directly plotted by experts' knowledge, while the deterministic method uses a variety of physical-based slope stability analyses with the aid of GIS [11]. One example of the latter is the expert opinion model for landslide susceptibility, developed by the Department of Geological Survey and Mineral Exploration (DGSE) in 2015 [12]; however, its accuracy has not been assessed and it was not intended for new urban development. Further, the deterministic method requires a significant amount of in situ tests and laboratory data. In contrast, the probabilistic statistical method combines parameter maps showing the possible causal factors of landslides and then calculates the weight of such maps statistically. As in situ testing and laboratory data were not available for the Hakha City landslides, this study selected the probabilistic statistical method for developing landslide susceptibility mapping before and after urbanization. Figure 1 depicts the second-largest landslide in Hakha City, which transpired at Mt. Rung.



**Figure 1.** Hakha City: The second-largest landslide in Hakha occurred at Mt. Rung (2299 m above sea level), covering 0.39 km<sup>2</sup> and affecting the Myohaung Quarter.

## 2. Materials and Methods

The methodological framework of this study consisted of three steps. Step 1 involved acquiring and processing the data; Step 2 focused on creating the landslide susceptibility maps; and Step 3 involved evaluation of the potential susceptibility of landslides and providing decision support for urban development. A flowchart depicting the research steps in detail is shown in Figure 2.

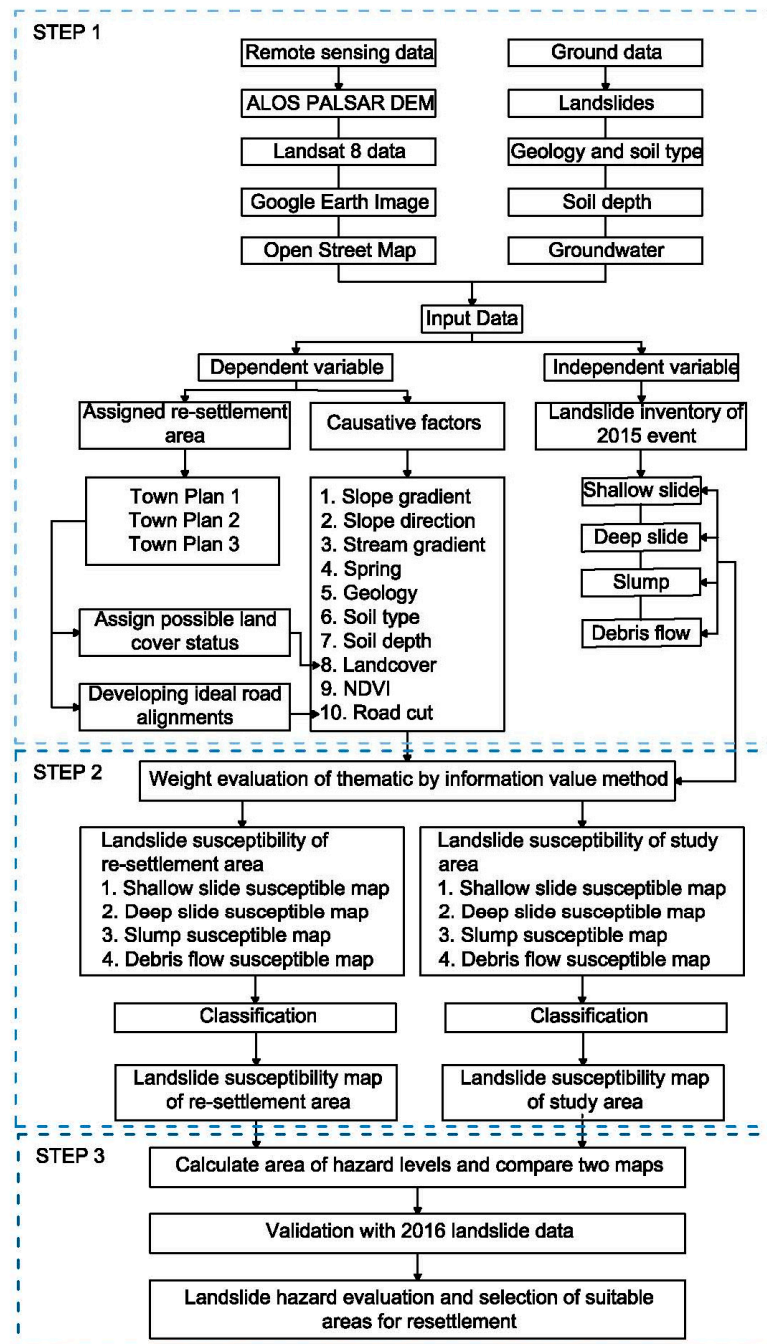
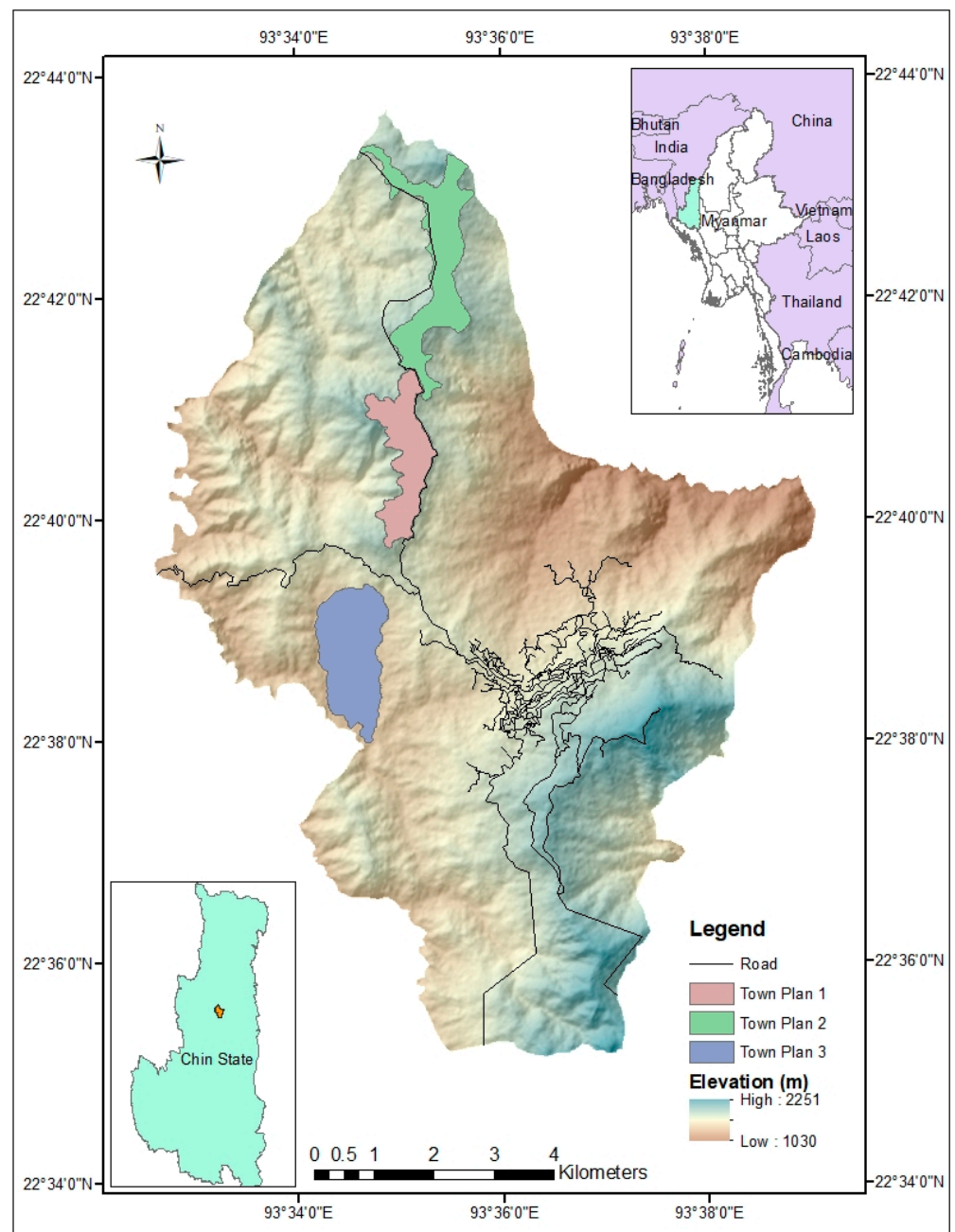


Figure 2. Flowchart of generating landslide susceptibility model for urban development.

Step 1 in the data collection for the landslide susceptibility map was to allocate the study area and create a Town Plan map (Figure 3). Data were obtained through field collection and lab testing, and from remote sensing images. For the statistical modeling of landslide susceptibility mapping, the landslide inventory map was assigned as the independent variable, and 10 parameter maps were assigned as the dependent variables.



**Figure 3.** Study area and proposed Town Plan map; Hakha City, Chin State, Myanmar. The study area, Town Plan, and road plan are assigned by the Chin State Government and data from the 12.5 m ALOS PALSAR DEM were applied.

The field data collection process began with creating a landslide inventory map as the independent variable. GPS technology was used to record landslide locations, and satellite images (Google Earth Pro), with a resolution of 0.2 m Airbus data and 30 m Landsat data of before and after the landslide affected the study area from its portal, respectively, were also utilized to identify landslides. Field measurements were conducted to supplement satellite data, including recording the location and dimensions of landslides, their types, groundwater conditions, land cover, and vegetation density. The collected data were used to create a categorized landslide inventory map (Figure 4).

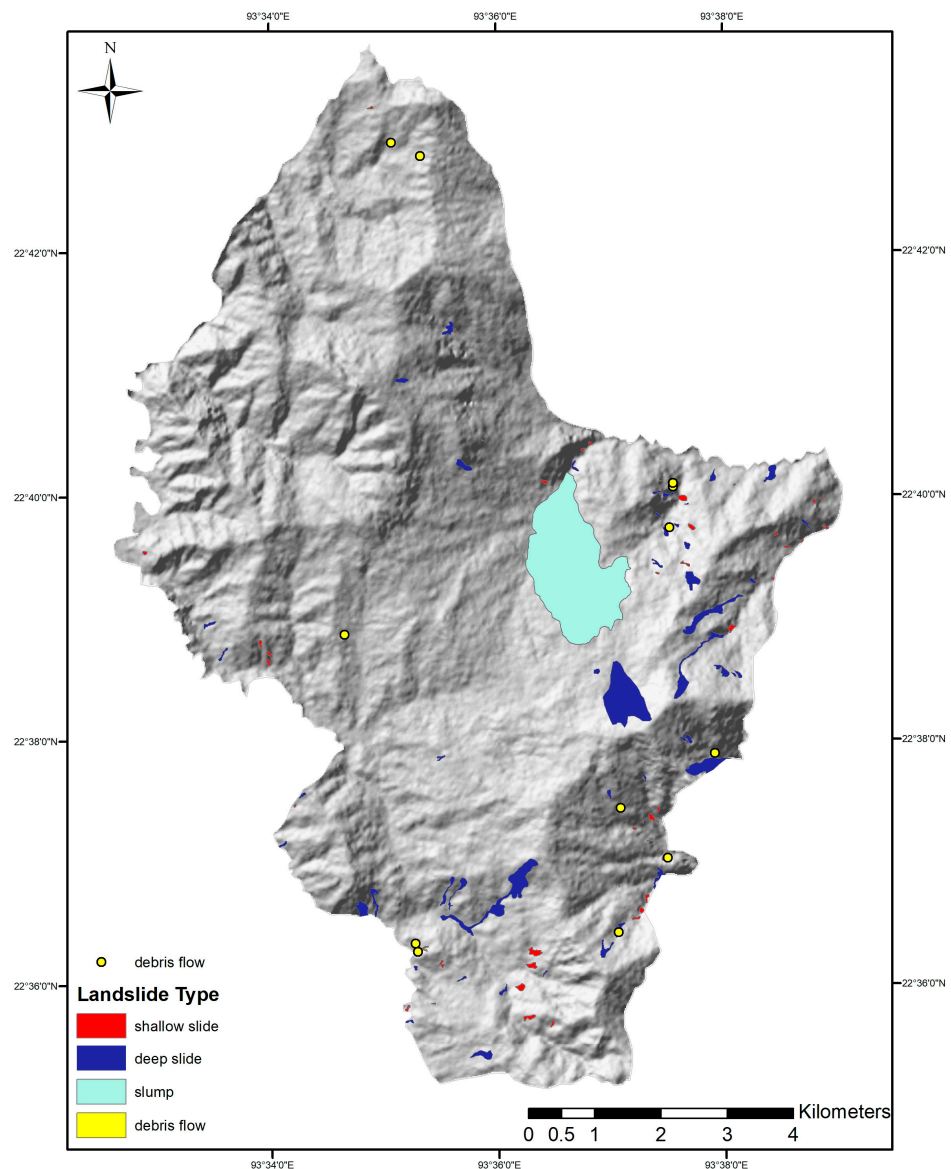


**Figure 4.** Landslide inventory map of Hakha City. The area coverage of debris flow was too small to show as a point feature.

Along with landslide records, the visual identification of natural vegetation density and land-cover type were recorded. Field geological data were collected for the purpose of generating a geological map and surface-soil distribution map. In addition, hydrogeological data, such as the locations of springs and their seasonal fluctuation, were collected and prepared as a seepage map. Finally, soil samples were also collected and tested to identify the engineering and physical properties of the subsurface.

The slope direction, slope gradient, and location of streams (drainage features) were extracted from the 12.5 m digital elevation model (DEM), acquired from the Phased Array type L-Band Synthetic Aperture Radar (PALSAR) sensor from the Advanced Land Observing Satellite (ALOS). Radiometric terrain correction was used to correct PALSAR data and present them as GeoTIFF data. All satellite data were downloaded from Alaska Satellite Facility Services [11]. Further, the thematic data layer of slope gradient and slope aspect (slope direction) were extracted by using a GIS three-dimensional analysis tool. Along with slope and aspect, the drainage pattern was extracted from the ALOS-PALSAR DEM.

Debris flows resulting from landslides are typically caused by the erosion of streams due to their velocity and runoff magnitude. The distance from the streams and their

gradient are critical factors in the formation of debris flows. To analyze this relationship, the drainage pattern was extracted through the use of a hydrology tool in a GIS spatial analysis. The distance from streams was divided into four classes, which were then overlaid with five classes of slope gradient to create a drainage map with a slope gradient thematic layer consisting of sixteen classes. This layer aids in a better understanding of the relationship between the drainage pattern and slope gradient, which is crucial for determining the likelihood of debris flow formation.

Notably, the natural springs and seepage were regarded as causal factors of rain-induced landslides. During a rainstorm, the rapid rise of groundwater reduces the shear strength of the slope to induce deep-seated landslides. In this study, the location of seepage was recorded while conducting the geological survey. Figure 5 shows the maps of slope gradient, slope aspect, the drainage of the slope gradient, and the distance from seepage.

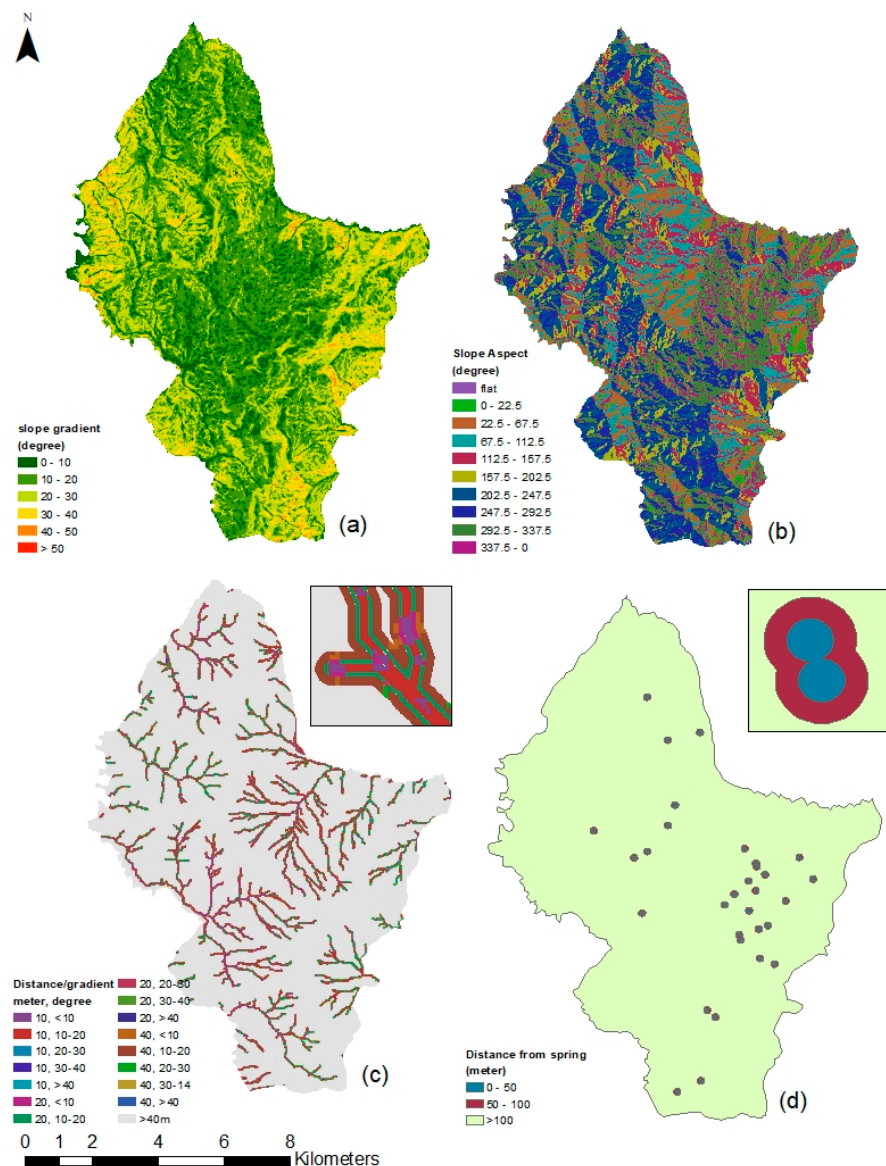


**Figure 5.** Parameter maps for statistical modeling: (a) slope gradient map; (b) slope aspect map; (c) map of drainage with respect to slope gradient map; (d) map of the distance from seepage.

The detailed survey for the geological map of Hakha City was conducted by DGSE in 2015. The data for the soil distribution map and soil depth map were collected via field survey with the aid of a GPS. The soil type was classified in the field and laboratory in accordance with the standard of the American Society for Testing and Materials, with

reference to ASTM D-2487–11: Standard practice for classification of soils for engineering purposes (Unified Soil Classification System). The soil depth was determined from the landslide scars, road cut, and stream cut with the aid of a tape and distance meter, and the soil depth map results were obtained via multi-criteria modeling.

Additionally, 30 m resolution Landsat 8 data were obtained from the United States Geological Survey website and used to map the land cover and vegetation density. The pixel-based supervised image classification method was utilized to differentiate between the land-cover classes. Before performing image classification, the number of land-cover classes had to be determined, which were identified during the field data collection process. In total, six land-cover classes were assigned to the study area. Of the 11 bands available in Landsat 8, the surface reflectance of the green (Band 3), red (Band 4), and near-infrared (NIR) (Band 5) bands were combined and then subjected to supervised classification using. Figure 6 depicts the maps of soil distribution, geology, optimal soil depth, and land cover. The normalized difference vegetation index (NDVI) map was generated by band ratioing the surface reflectance data of the NIR (Band 5) and red (Band 4) bands from the Landsat 8 dataset [13,14]. The NDVI is widely used as vegetation density for landslide study [15,16].

The road network in the Hakha Area was extracted from Open Street Map; however, an updated version of the road network was digitized from Google Earth. The distances from the road network with respect to the slope gradient were created by buffering distances from the road alignment and classifying them based on slope gradients. The parameter maps of NDVI and the distance from the road alignment with respect to the slope gradient are depicted in Figure 7. Table 1 lists the parameter maps and their sources of acquisition.

**Table 1.** List of parameter maps and their source of acquisition for the landslide susceptibility map statistical modeling.

No.	Parameter Map	Sources
1.	Slope gradient	ALOS PALSAR DEM
2.	Slope direction	ALOS PALSAR DEM
3.	Distance from stream	ALOS PALSAR DEM
4.	Distance from seepage	Ground survey
5.	Soil distribution	Ground survey and laboratory tests
6.	Geological	Ground survey
7.	Soil depth	Ground survey and modeling
8.	Land cover	Landsat 8
9.	NDVI	Landsat 8
10.	Distance from the road network	Open Street Map, Google Earth
11.	Landslide inventory	Google Earth, ground survey

The Chin State Government selected three potential resettlement areas, but the risk from natural disasters has yet to be evaluated. All three areas have different land-cover types; meanwhile, this can be changed by urban development and be affected, both positively and negatively, by disaster risk. To assess the degree of impact, 2 of the 10 parameter maps for landslide susceptibility were changed to reflect potential changes after urbanization (Figure 8). Theoretically, it is possible to change all parameters after urbanization, and such changes could be measured after the development of a detailed urbanization plan. Yet, in the preliminary investigation stage, only 2 out of 10 parameters—land cover and road network—will be significantly changed. Therefore, in this study, the existing natural landscape in the land-cover map and road network map was substituted with the urban thematic class and distance from the road with respect to the slope gradient.

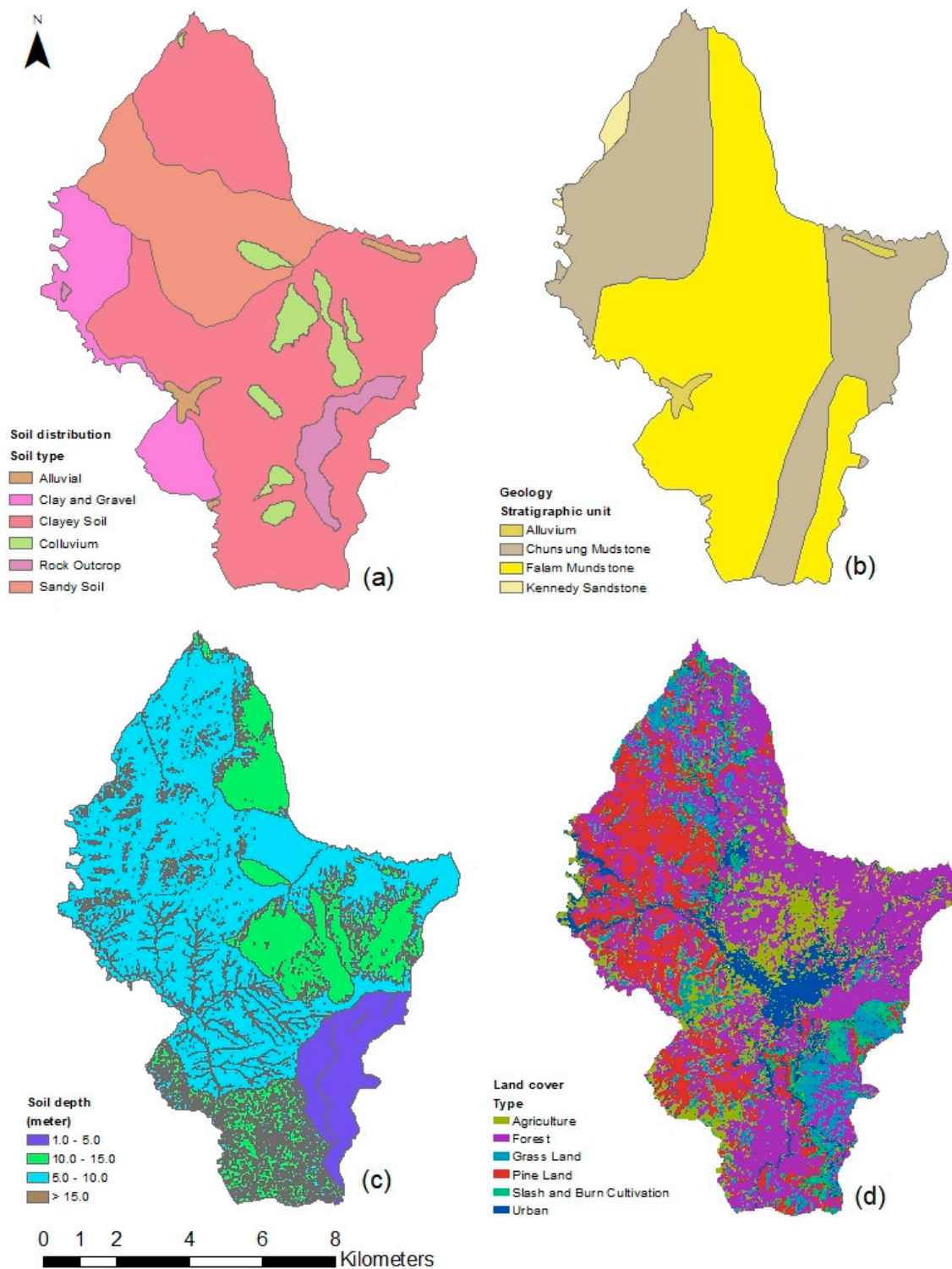


**Figure 6.** Parameter maps of statistical modeling: (a) soil distribution map; (b) geology map; (c) optimum soil depth map; (d) land-cover map.

After Step 1 of data acquisition and processing the parameter maps for the independent and dependent variables, Step 2 generated the landslide susceptibility maps. The landslide susceptibility map should indicate existing or potential landslides, showing their type, volume or area, and spatial distribution. Using a bivariate statistical method known as information value analysis (IVA), the weight of each thematic layer was calculated from the

dependent (landslide distribution and size) and independent (slope, geology, soil depth, etc.) variables to determine potential landslide zones.

IVA is a bivariate statistical method for spatial prediction of the potential landslide that is based on the relationship between the previous landslide occurrence and controlling parameters of the landslide [17–19]. GIS-based IVA can be applied for generating the landslide hazard zonation map by estimating the regional probability of landslide occurrence within each thematic class [11,20–22]. The class density is calculated by finding the area of each class where landslides have occurred, and dividing it by the total area of that class on the map. The information value of a class is determined by considering the log value of the ratio of the probability of a landslide occurring in that class, given past occurrences, to the overall probability of a landslide in that area [17,23]. The weight of a class in a thematic is determined by Equation (1):

$$W_i = \ln \left[ \frac{D\_Class}{D\_Map} \right] = \ln \left[ \frac{(Area\_Is / Area\_tmc)}{(TArea\_Is / TArea)} \right] \tag{1}$$

where  $W_i$  is the weight of a certain class in the parameter map,  $D\_Class$  refers to the landslide density within a parameter class,  $D\_Map$  = the landslide density within the entire parameter map,  $Area\_Is$  = area of landslide in a certain class, and  $Area\_tmc$  = total area of a certain class in a parameter map,  $TArea\_Is$  = total area of landslide in a study area,  $TArea$  = total study area.

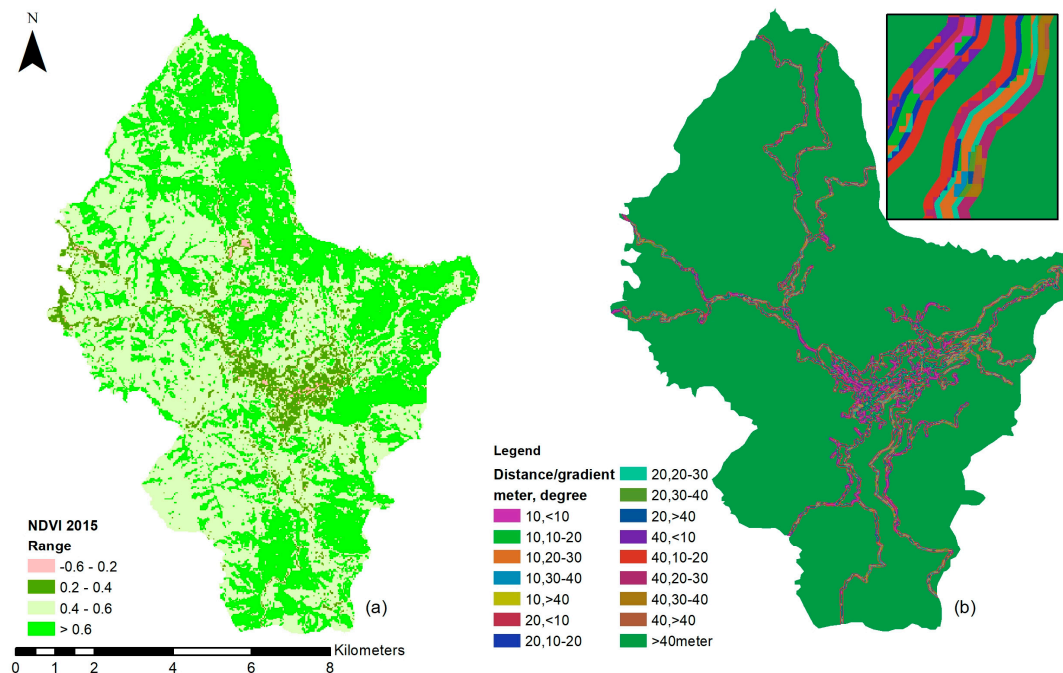


**Figure 7.** Parameter maps of statistical modeling 3: (a) NDVI map; (b) distance from road with respect to slope gradient map.

The area of each thematic class contained in the landslide area ( $D\_Class$ ) was extracted from 10 thematic maps by clipping analysis with area coverage of landslides from the landslide inventory map. As the landslide susceptibility was separately conducted in accordance with the landslide type, the extraction of  $D\_Class$  was carried out for four types of landslide. Thus,  $D\_Map$  represents the total area coverage of the thematic class in a thematic map,  $TArea\_Is$  is the total area coverage of landslides in a specific type, and  $TArea$  is the total area coverage of the study area. GIS tools supported the area extraction and calculation process in this operation. Table 2 indicates the weighted values for the thematic classes within parameter maps for four landslide types.

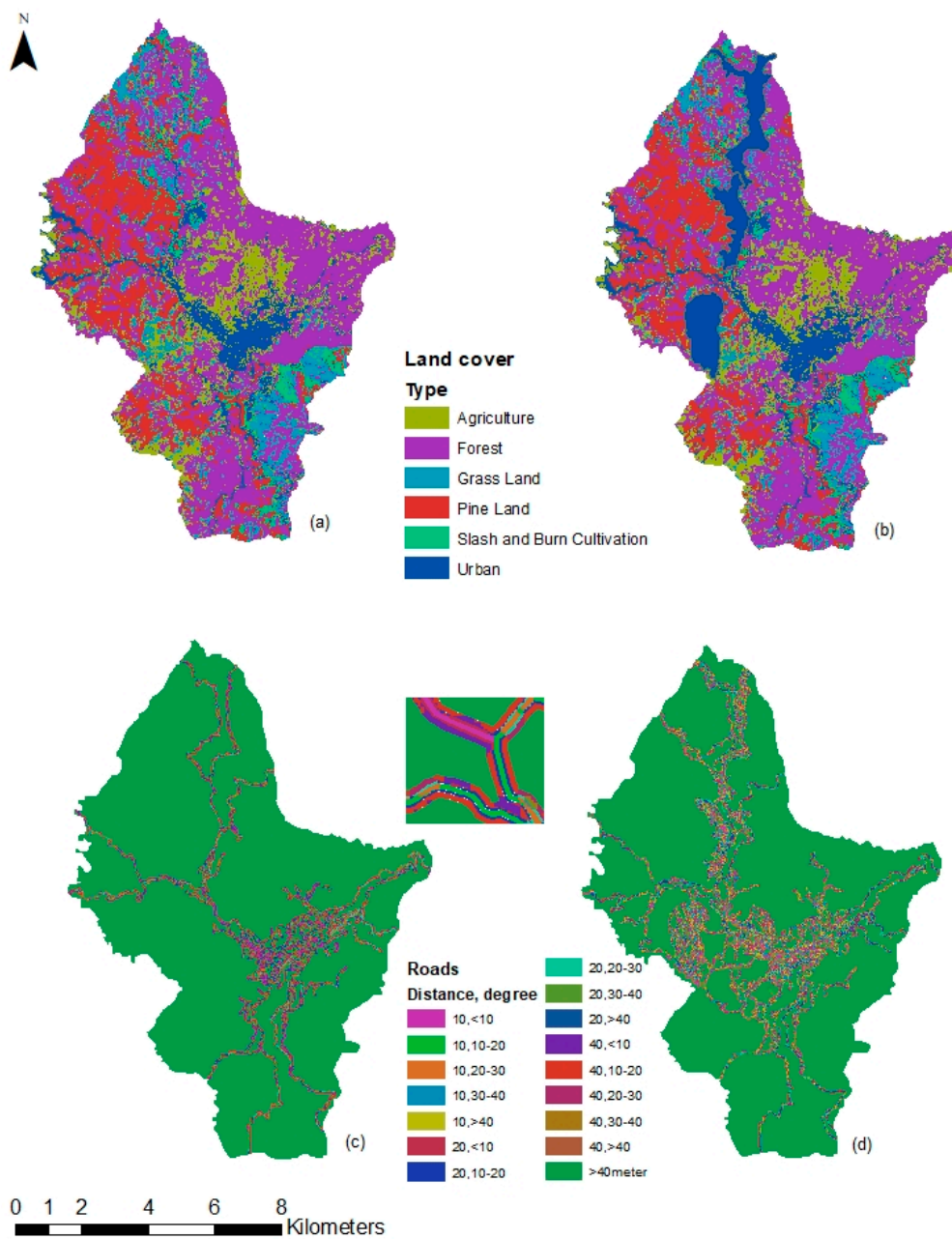


**Figure 8.** Thematic maps of land cover and road networks before and possible changes after urbanization: (a) land-cover map before urbanization; (b) land cover after urbanization; (c) road network with respect to slope before urbanization; (d) road network with respect to slope after urbanization.

**Table 2.** List of weighted values for thematic classes of parameter maps.

Layer (Parameter Map)	Thematic Layer	Information Value (Weight)			
		Shallow Slide	Deep Slide	Slump	Debris Flow
Slope gradient (degree)	0–10	−1.75	−0.60	0.58	−0.44
	10–20	−0.79	−0.54	0.35	−0.06
	20–30	0.50	0.37	−1.19	0.26
	30–40	0.99	0.85	−2.88	−0.20
	40–50	1.62	0.72	−6.42	−0.50
	>50	0.00	0.00	−3.87	0.21

Table 2. Cont.

Layer (Parameter Map)	Thematic Layer	Information Value (Weight)			
		Shallow Slide	Deep Slide	Slump	Debris Flow
Slope aspect (degree)	Flat (−1)	0.00	−0.67	−0.87	0.00
	North (0–22.5)	−0.74	0.20	0.83	−0.12
	Northeast (22.5–67.5)	−0.79	0.27	−0.30	0.25
	East (67.5–112.5)	0.04	−0.50	−2.78	0.45
	Southeast (112.5–157.5)	0.67	−0.51	−4.13	−0.03
	South (157.5–202.5)	0.45	−0.15	−5.27	−1.47
	Southwest (202.5–247.5)	−0.06	−0.09	−4.01	−0.26
	West (247.5–292.5)	0.39	−0.57	−0.81	0.74
	Northwest (292.5–337.5)	−0.67	0.50	1.08	−0.77
	North (337.5–360.0)	−0.85	0.35	1.30	−2.75
Stream (distance/gradient) (m/degree)	10, <10	−0.84	0.43	0.54	−0.87
	10, 10–20	0.86	0.66	0.62	−0.67
	10, 20–30	1.46	0.76	−0.44	1.72
	10, 30–40	1.33	0.60	−0.56	0.00
	10, >40	0.00	0.00	0.00	0.00
	20, <10	−0.94	0.25	0.62	−1.22
	20, 10–20	0.38	0.48	0.64	0.00
	20, 20–30	1.62	0.70	−0.64	1.36
	20, 30–40	2.20	−0.51	−0.30	0.00
	20, >40	4.02	0.00	0.03	0.00
	40, <10	−2.31	0.12	0.86	−0.67
	40, 10–20	−0.16	−0.02	0.70	0.43
	40, 20–30	1.04	0.44	−0.77	0.42
	40, 30–40	2.26	−0.46	−1.89	−3.47
	40, >40	3.84	0.00	−5.28	0.00
Spring (m)	>40	−0.15	−0.08	−0.13	−0.04
	0–50	0.79	2.65	1.84	0.00
	50–100	−0.90	2.19	1.74	0.00
Soil type	>100	0.00	−0.11	−0.06	0.01
	Colluvium	−0.05	2.13	2.20	0.00
	Rock outcrop	−2.37	−0.87	0.00	0.00
	Alluvial	−1.53	−0.60	0.00	0.00
	Clayey soil	0.12	−0.19	−0.11	0.48
	Sandy soil	−0.39	−2.85	−3.94	0.00
Geology	weathered rock	0.18	−0.87	0.00	0.00
	Alluvium	−1.49	−0.56	0.00	0.00
	Kennedy Sandstone	0.00	0.00	0.00	0.00
	Chunsung Mudstone	0.41	0.09	−6.16	−0.44
	Falam Mudstone	−0.43	−0.04	0.58	0.26
Soil depth (m)	1.0–5.0	0.54	0.15	0.00	0.76
	5.0–10.0	−0.10	−1.03	−0.76	0.08
	10.0–15.0	−0.05	0.92	0.99	−0.85
	>15.0	2.50	0.98	0.00	0.00
Land cover	Agriculture	−1.10	−1.13	0.35	−0.50
	Grass land	0.23	0.82	−4.26	0.72
	Urban	0.87	−0.18	0.60	−0.69
	Forest	0.54	1.03	0.05	0.92
	Pine land	−0.29	−1.85	−4.85	−2.99
NDVI	Slash and burn cultivation	0.23	−1.35	0.00	−0.25
	−0.6 to 0.2	−6.66	−2.48	−2.65	0.00
	0.2–0.4	−0.97	−2.01	−0.49	0.00
	0.4–0.6	−0.01	−0.74	0.24	−0.48
Road (distance, slope) (m, degree)	>0.6	0.49	1.11	−0.27	1.04
	10, <10	0.00	−0.85	1.17	0.71
	10, 10–20	−2.15	−0.98	1.04	0.81
	10, 20–30	1.37	0.39	0.30	1.36

Table 2. Cont.

Layer (Parameter Map)	Thematic Layer	Information Value (Weight)			
		Shallow Slide	Deep Slide	Slump	Debris Flow
	10, 30–40	2.15	0.48	−0.82	0.00
	10, >40	0.00	2.10	0.00	0.00
	20, <10	0.00	−0.69	1.15	0.72
	20, 10–20	−2.96	−0.87	1.08	0.77
	20, 20–30	1.36	0.50	0.15	1.51
	20, 30–40	2.05	0.54	−1.48	0.00
	20, >40	0.00	1.54	0.00	0.00
	40, <10	0.00	−0.58	1.18	1.20
	40, 10–20	−3.30	−0.55	1.14	0.88
	40, 20–30	1.23	0.55	−0.05	1.33
	40, 30–40	1.88	0.61	−1.70	0.00
	40, >40	0.00	0.69	0.00	0.00
	>40	−0.06	0.02	−0.19	−0.24

The class was assigned based on the resulting weights and was converted into raster maps to generate landslide susceptibility maps, using the GIS raster overlay method. The hazard level was then classified based on the IVA scheme [24]. Separate susceptibility maps were generated for each landslide type, as the mitigation plans can be expected to differ.

Furthermore, the possible changes of land cover and landscape in resettlement areas were mapped using the same process of calculation as in the first procedure (Figure 8). The overall landslide susceptibility of Hakha City was developed using the statistical IVA model and the same classification scheme.

Step 3 extracted the landslide susceptibility before and after urbanization for three Town Plans and calculated the area coverage of the degree of susceptibility using a GIS tool, and compared increasing or decreasing degrees of susceptibility. The landslide susceptibility models of before and after urbanization were developed based on 2015 landslide inventory data. The accuracy of the model was then verified using 2016 landslide data. The areas of different hazard levels from the susceptibility maps before and after urbanization were calculated and compared.

### 3. Results

#### 3.1. Landslide Susceptibility Pre-Urbanization

The study area's landslide inventory was created by extracting the distribution and dimension data from the satellite images. Field data collection was used to identify the types of landslides and their modes of failure, including the detection and mapping of hidden landslides that mostly occur in urban areas where land cover is mixed and modified. According to a previous classification of subaerial slope movement [25], the landslides in the Hakha Area can be categorized into four types: shallow slides, deep slides, slumps, and debris flows. The preliminary investigation showed that shallow earth slides are caused by excessive soil moisture, whereas deep slides are a result of rising groundwater levels [12,26,27]. The largest landslide in the area, a slump, was observed on a gentle gradient where colluvium had been deposited. This type of landslide was primarily caused by a combination of excessive soil moisture, rising groundwater levels, and erosion of the slope toe by running water [12,26,27]. Further, debris flows were formed by the erosion and transportation of stream flow [12,26]. Overall, the main trigger factor for all landslides was found to be rainfall. Out of the 112 total landslides in over 3.63 km<sup>2</sup>, 51 shallow landslides covered 0.15 km<sup>2</sup>, 48 deep landslides covered 1.17 km<sup>2</sup>, 1 slump covered 2.29 km<sup>2</sup>, and 12 debris flows covered 0.02 km<sup>2</sup>.

Table 2 indicates the weight for each thematic class, calculated by IVA, in 10 thematic maps, which was applied to the parameter maps to facilitate landslide susceptibility mapping.

The information values in the above table were assigned to each thematic layer in 10 parameter maps and overlaid with raster maps using the weighted average overlay method. As the study area comprised four different landslide types, the susceptibility is shown in four maps. Each pixel contains a landslide susceptibility index, from which the map was classified into five classes according to the information value classification scheme to depict landslide susceptibility (Figure 9).

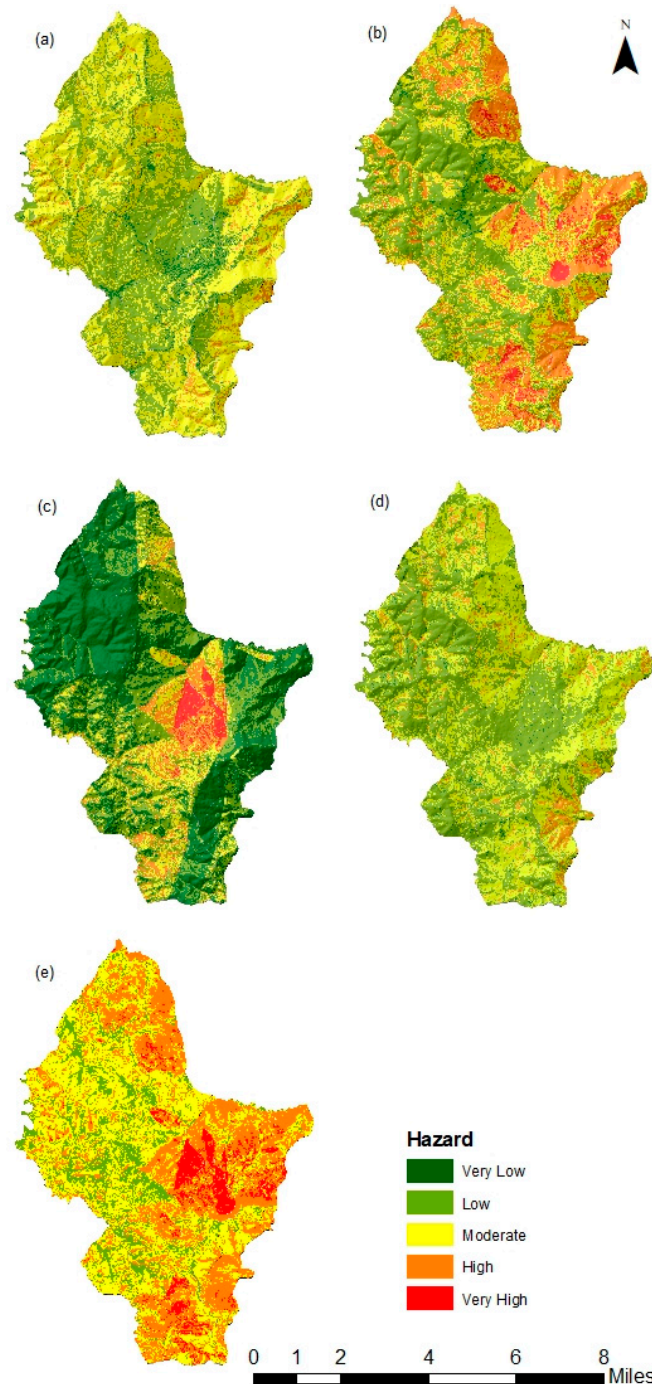


**Figure 9.** Landslide susceptibility maps of the Hakha Area generated by information value modeling: (a) shallow slide; (b) deep slide; (c) slump; (d) debris flow; (e) overall landslide susceptibility.

The accuracy assessment of landslide susceptibility was calculated by AUC (area under the curve) [2,3,28]. The AUC shows the success rate, plotting the percentage of the susceptibility indices ordered from the highest to lowest values against the percentage of

the landslide. The success rate is a statistical method to determine how well the resulting susceptibility map has predicted the areas of existing landslides as high-hazard areas [11]. The AUC of the information value model was calculated at 80.67% and that of the standard error at 0.0689.

### 3.2. Landslide Susceptibility Post-Urbanization

The modeling results indicate that the level of landslide susceptibility increased in all selected areas after urbanization. In Town Plan 1, 10% of the total area (141,875 m<sup>2</sup>) was found to have high to very high susceptibility levels. In Town Plan 2, 16% of the total area (356,365 m<sup>2</sup>) had high to very high susceptibility levels. In Town Plan 3, 5% of the total area (12,239 m<sup>2</sup>) had high to very high susceptibility levels. Figures 10 and 11 compare the changes in landslide susceptibility of each landslide type, and Table 3 illustrates the changes in the degree of area coverage of landslide susceptibility in Town Plan 1. Figures 12 and 13 compare the changes in landslide susceptibility before and after urbanization in Town Plan 2, whereas Figures 14 and 15 compare that of Town Plan 3. The changes in the degree of landslide susceptibility in area coverage of Town Plans 2 and 3 are listed in Tables 4 and 5, respectively.

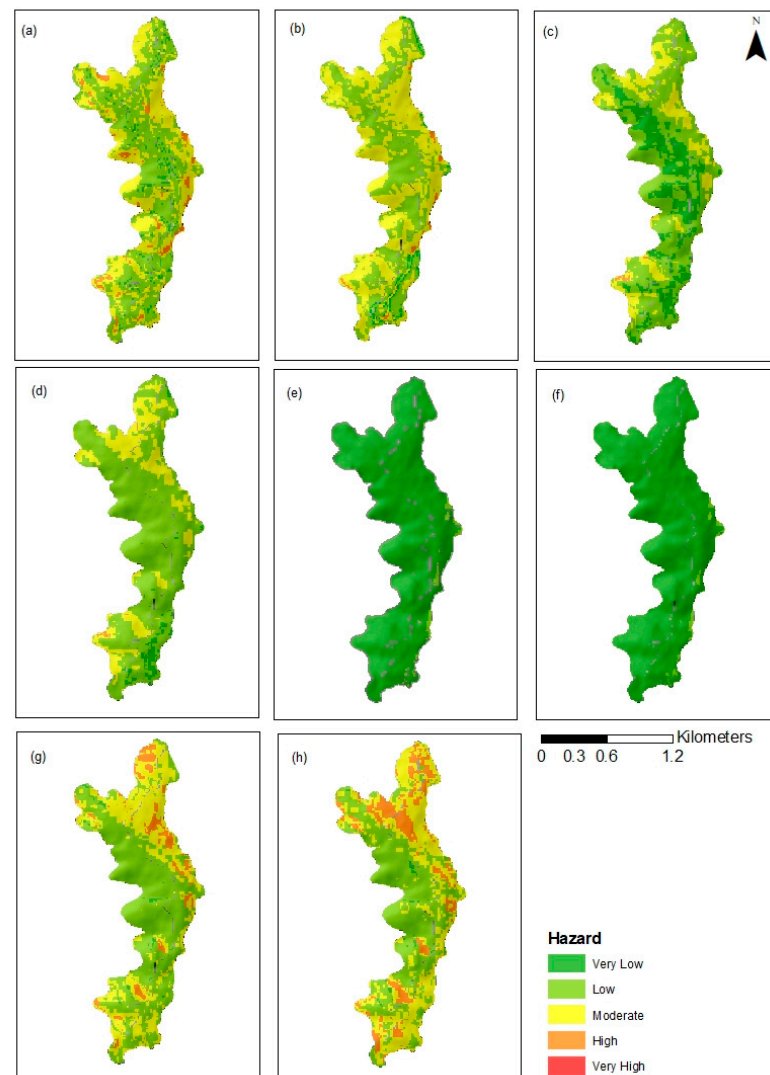


**Figure 10.** Changes in landslide susceptibility before and after urbanization in Town Plan 1: (a) shallow slide before and (b) after development; (c) deep slide before and (d) after development; (e) slump before and (f) after development; (g) debris flow before and (h) after development.

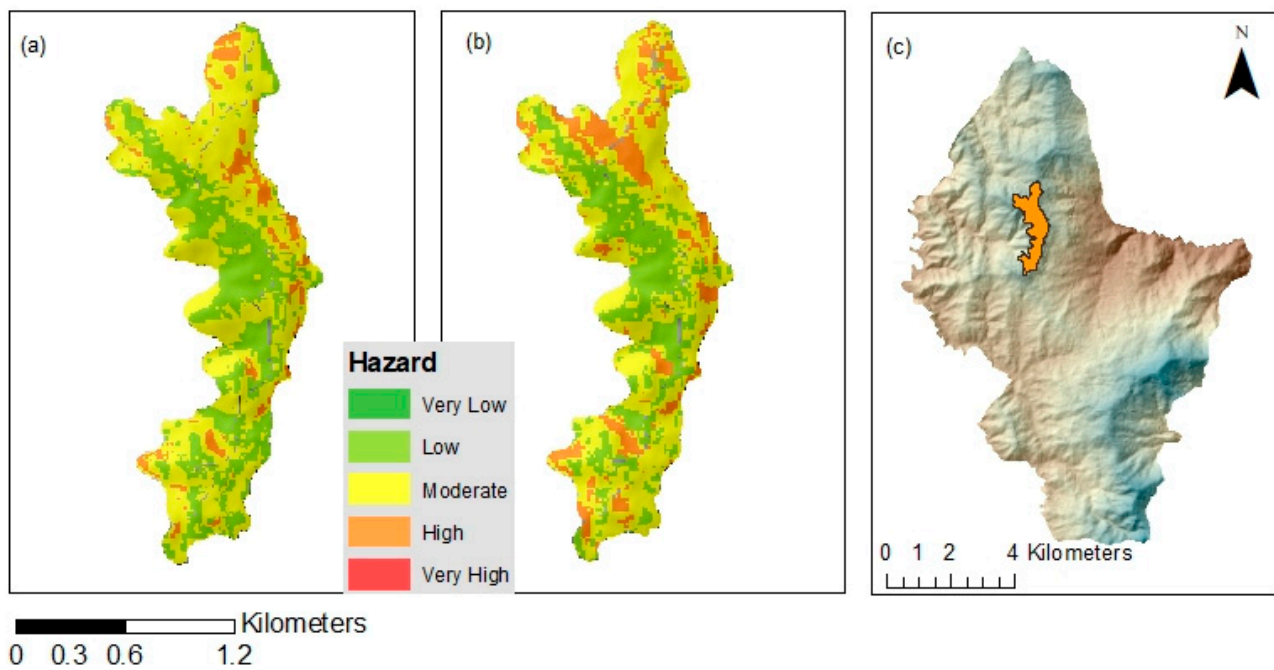


**Figure 11.** Changes in landslide susceptibility before and after urbanization in Town Plan 1: (a) landslide before and (b) after development; (c) location map of Town Plan 1.

**Table 3.** Changes in hazard level before and after urbanization in Town Plan 1.

Type	Timing	Very Low Area (m <sup>2</sup> )	Low Area (m <sup>2</sup> )	Moderate Area (m <sup>2</sup> )	High Area (m <sup>2</sup> )	Very High Area (m <sup>2</sup> )
Shallow slide	Before:	30,036	699,034	799,473	19,737	0
	After:	73,153	786,321	620,134	69,843	0
Deep slide	Before:	54,001	1,152,972	335,259	6047	0
	After:	353,632	921,389	269,064	5367	0
Slump	Before:	1,520,002	29,449	0	0	0
	After:	1842	26,437	0	0	0
Debris flow	Before:	14,080	894,448	532,939	106,812	0
	After:	12,099	733,879	582,227	221,021	225
All landslide types	Before:	0	538,620	881,660	127,999	0
	After:	0	455,547	824,030	269,649	225

**Table 4.** Changes in hazard level before and after urbanization in Town Plan 2.

Type	Timing	Very Low Area (m <sup>2</sup> )	Low Area (m <sup>2</sup> )	Moderate Area (m <sup>2</sup> )	High Area (m <sup>2</sup> )	Very High Area (m <sup>2</sup> )
Shallow slide	Before:	81,104	746,407	1,385,489	55,705	0
	After:	71,984	1,076,039	911,798	207,854	0
Deep slide	Before:	1623	768,948	893,545	587,136	16,423
	After:	1320	710,300	904,167	638,845	14,073
Slump	Before:	1,043,835	784,197	374,972	64,451	1250
	After:	953,501	821,535	390,028	100,811	1800
Debris flow	Before:	22,938	856,371	1,201,496	187,848	0
	After:	8008	624,575	1,120,472	514,621	0
All landslide types	Before:	1319	710,301	904,167	638,845	14,073
	After:	0	256,783	1,001,610	991,059	18,223

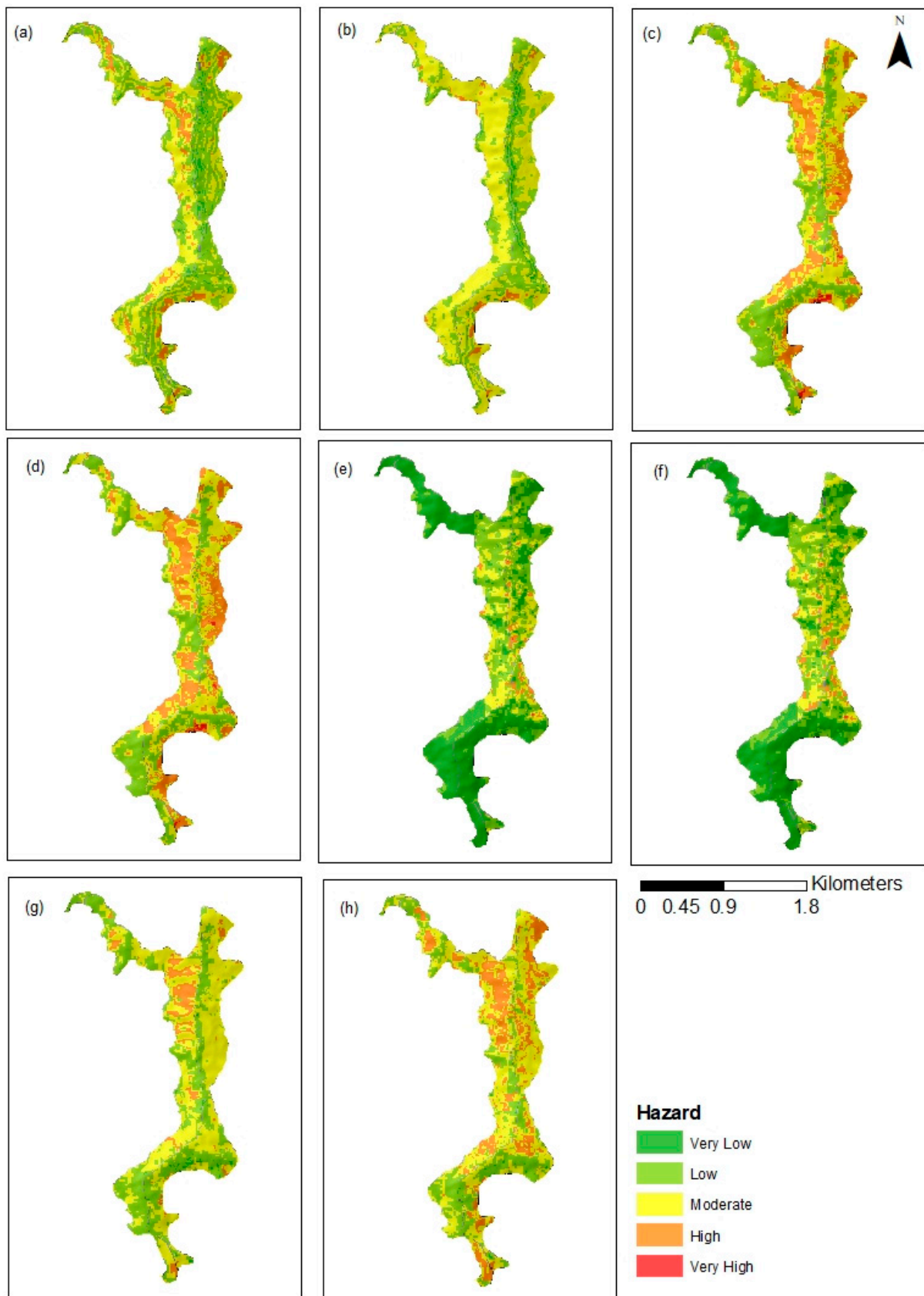


**Figure 12.** Changes in landslide susceptibility before and after urbanization in Town Plan 2: (a) shallow slide before and (b) after development; (c) deep slide before and (d) after development; (e) slump before and (f) after development; (g) debris flow before and (h) after development.

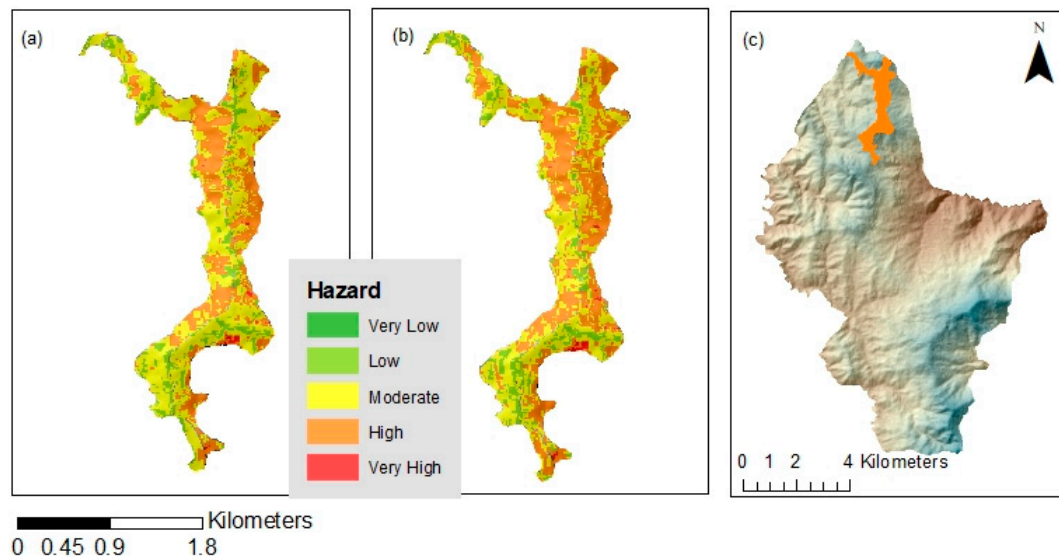


**Figure 13.** Changes in landslide susceptibility before and after urbanization in Town Plan 2: (a) landslide before and (b) after development; (c) location map of Town Plan 2.

**Table 5.** Changes of hazard level before and after developing urbanization in Town Plan 3.

Type	Timing	Very Low Area (m <sup>2</sup> )	Low Area (m <sup>2</sup> )	Moderate Area (m <sup>2</sup> )	High Area (m <sup>2</sup> )	Very High Area (m <sup>2</sup> )
Shallow slide	Before:	34,208	1,503,177	646,079	2187	0
	After:	255,800	1,461,052	444,457	24,750	0
Deep slide	Before:	4113	1,242,731	802,327	136,481	0
	After:	19,300	1,540,382	542,585	83,791	0
Slump	Before:	908,505	1,009,594	223,229	44,325	0
	After:	715,116	1,064,542	288,331	118,070	0
Debris flow	Before:	18,893	1,357,271	762,314	47,174	0
	After:	13,680	1,114,673	917,397	140,309	0
All landslide types	Before:	0	933,535	1,054,640	197,477	0
	After:	0	801,143	1,065,198	319,717	0

It was observed that the potential for deep slides decreased after urbanization in Town Plans 1 and 2. This can be attributed to the fact that the statistical model used in this study is evidence-based and considers past landslide events in urban areas. The model suggests that fewer landslides occurred in existing urban areas compared to forest and grassland areas due to the presence of retaining structures in urban areas. The conversion of forest and grassland areas to urban areas in Town Plans 1 and 2 resulted in a decrease in information values and a reduction in the potential for deep sliding. Similarly, the potential for slumps was generally low in Town Plan 1 after urban development. In the study area, one large area of a single slump occurred on a gentle slope gradient (less than 20°) with a thickly deposited soil layer (more than 6 m). Town Plan 1 was characterized by moderate to steep slopes (20° to 50°) and generally had a soil thickness of less than 6 m, which reduced the potential for slumping. However, the potential for slumps increased in Town Plans 2 and 3 after urbanization. The modeling results indicate that shallow slide and debris flow risks would increase after urbanization in all areas.

According to the results, Town Plan 3 is the most suitable resettlement area due to the low risk of landslides, followed by Town Plans 1 and 2. This is because the results show that landslides affected Town Plans 1 and 2 during the 2016 rainy season. Shallow landslides, including tension cracks, occurred in the northern part of Town Plan 1 on 2 August 2016. Before urbanization, the landslide susceptibility was moderate, and after

urbanization, it was moderate to high. In Town Plan 2, a shallow landslide also occurred on 12 June 2016, with a susceptibility ranging from very low to high before urbanization, and low to high after urbanization. Figure 16 presents the results of the potential landslide susceptibility modeling for urbanization and the locations of landslides in 2016. Figure 17 displays photographs of landslides in Town Plans 1 and 2 during the rainy season of 2016.

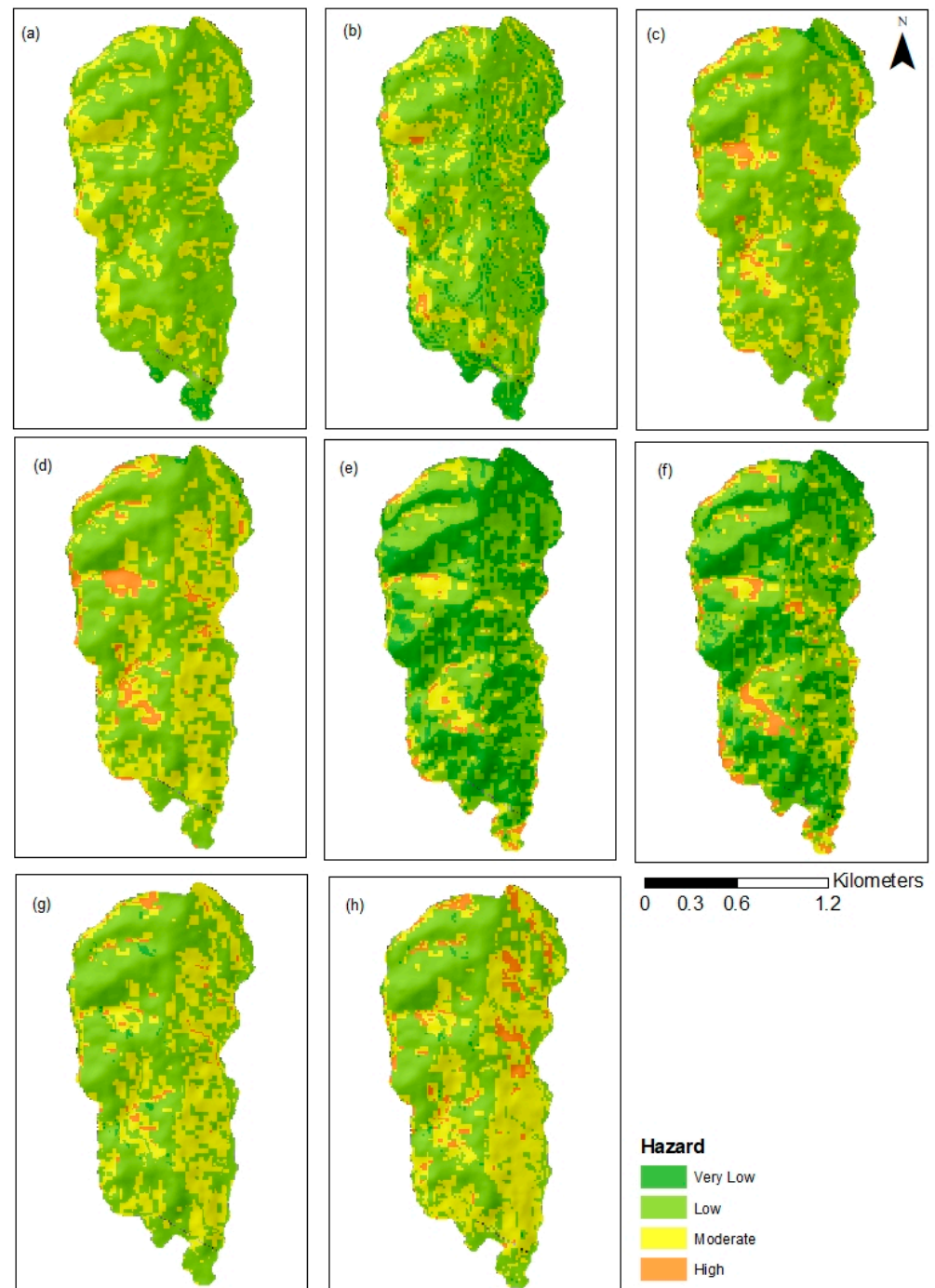


**Figure 14.** Changes in landslide susceptibility before and after urbanization in Town Plan 3: (a) shallow slide before and (b) after development; (c) deep slide before and (d) after development; (e) slump before and (f) after development; (g) debris flow before and (h) after development.

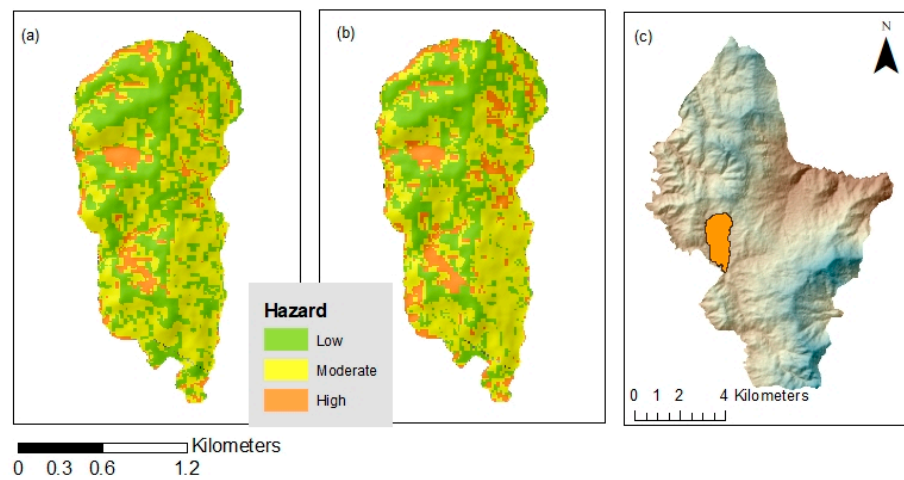


**Figure 15.** Changes in landslide susceptibility before and after urbanization in Town Plan 3: (a) landslide before and (b) after development; (c) location map of Town Plan 3.

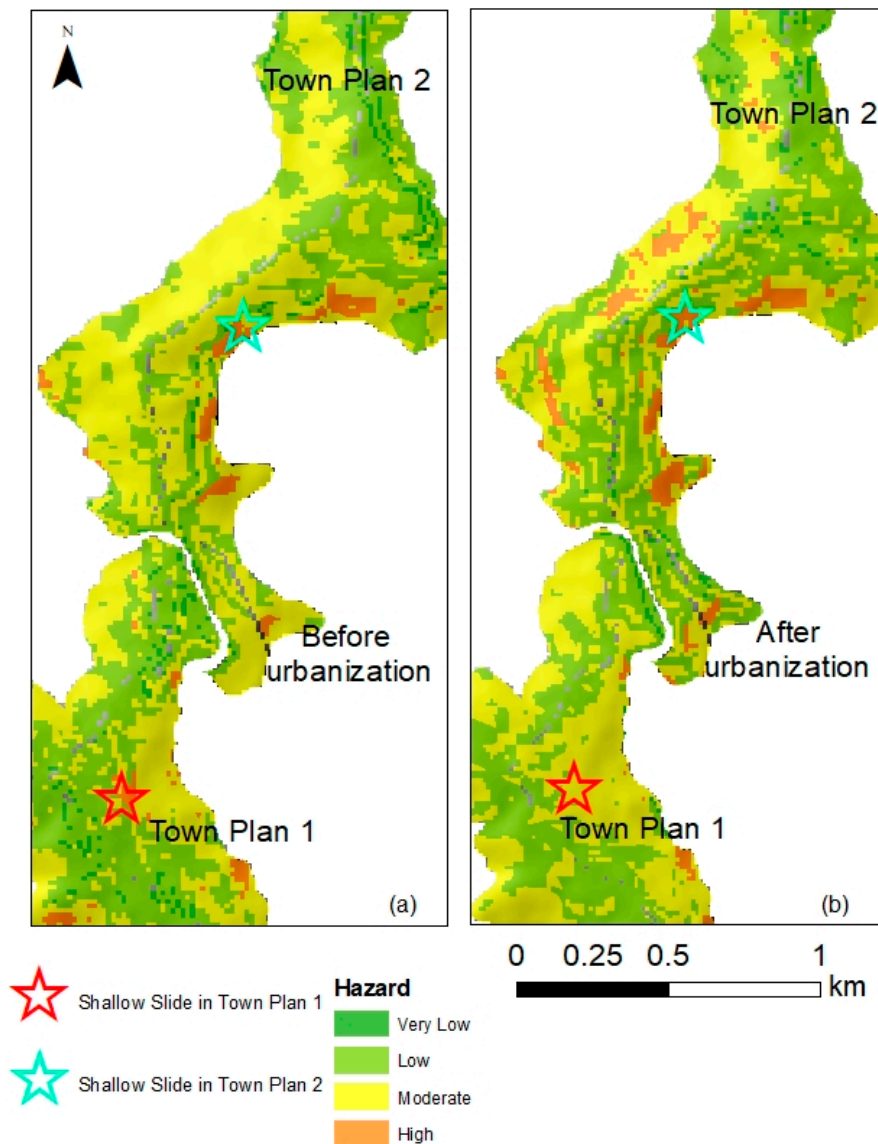


**Figure 16.** Shallow slide susceptibility maps of Town Plans 1 and 2, (a) before and (b) after urbanization, and location of landslides (shallow slides) in 2016.



**Figure 17.** Landslides (shallow slides) occurred in the newly developed urban area of (a) Town Plan 1 and (b) Town Plan 2. Town Plans 1 and 2 were immediately implemented as resettlement areas for affected residents in Hakha City. Source: Hakha Rescue Committee.

### 3.3. Discussion

The landslides, particularly shallow slides and deep slides, increased gradually as the slope angle increased up to  $50^\circ$  in Hakha; however, no landslides occurred when the slope angle exceeded  $50^\circ$ . Kennedy Sandstone, which is thickly bedded with high resistance, rests at steep slopes, generally has a slope gradient higher than  $50^\circ$ , and is at a very low risk of landslide. Notably, the largest landslide of earth slump formed at a lower elevation on a gentle slope gradient between  $10^\circ$  and  $20^\circ$ .

According to the IVA of landslides in the Hakha Area, the slope direction is not correlated with landslides. Shallow slides commonly occurred on south-facing slopes, while slides, slumps, and debris flows occurred on north-facing slopes. In Chin State, monsoons arrive from the southwest and directly impact south-facing slopes, often causing shallow slides.

According to the statistical analysis of landslide susceptibility, areas where the drainage distance was between 0 and 40 m had a high probability of landslides. As the slope gradient controls the velocity of discharge, the probability of a shallow slide increases with the increase in slope gradient along the stream section. Additionally, the formation of debris flows increased with an increase in the slope gradient where the drainage distance was less than 40 m; however, they did not form where the slope gradient exceeded  $40^\circ$ . Although there is some evidence of deep slides and a slump occurring within 20 m of streams, our IVA did not find a strong correlation between the stream and slope gradient.

According to field observations, seepages and natural springs were commonly observed in the larger landslide areas. Fluctuations in groundwater levels have been shown to reduce the effective intergranular pressure and friction, thereby increasing capillary tension and reducing the shear strength of the soil and rock materials at the slope, as reported in a previous study [29]. In this study, statistical analysis indicates that the occurrence of deep slides and slumps is strongly correlated with springs, while the relationship between shallow slides and springs is only slightly correlated. However, no correlation was found between debris flows and springs or seepages.

During field investigation, landslides were likely to be found in the Falam Mudstone and Chunsung Mudstone areas. Our analysis supports the findings that shallow slides are abundantly distributed in Chunsung Mudstone, while debris flows and slumps are commonly observed in Falam Mudstone. Additionally, the flat-lying alluvial plains are considered to be landslide-free areas. As the study area is largely covered by residual soils, alluvium, colluvium, and weathered rock, which have a granular soil-like nature, the formation and depth of the soil constitute a more significant controlling factor for landslides than is the rock type in the area.

As the study area is commonly covered with soil and thick weathered rocks, most landslides were attributed to soil slope failure and debris failure. According to our study, there is a high probability of landslides occurring in colluvium-rich areas—made up of clayey sand with abundant gravel; the two largest landslides, the Mt. Rung Slide and Myohaung Quarter Slump, were formed as such. Although debris flows frequently initiate as shallow slides and deep slides in upland areas, they tend to be deposited in lower elevation areas where sandy and clayey soils are present. The loose nature of the colluvium soil grains results in an increased likelihood of slump formation. Shallow slides are abundant in steep slope areas where clay-dominated residual soil and weathered rock are present.

Soil depth and subsurface flow play an important role in shallow landslide mechanisms [30]. However, in this study, the soil depth was found to significantly control the formation of deep landslides; the higher the depth of soil, the higher the risk of deep slides and slumps occurring. We suggest that the Myohaung Quarter Slump formed due to the presence of a more than 10-m-thick colluvial deposit. Nevertheless, soil depth did not impact the formation of shallow slides or debris flows in the study area.

Numerous studies have shown that shallow landslides are significantly impacted by changes in land use or land cover [26,31–35]. In the study area, shallow landslides are predominantly distributed in urban areas where vegetation cover is sparse or absent and the landscape has been modified for construction purposes. However, shallow landslides are also commonly observed in forest and grassland areas with dense vegetation. Debris flows followed by slides have been observed in forested and grassland areas, while a major landslide slump is prevalent in the Myohaung Quarter, with a mixture of urban areas and agricultural farms. The dense vegetation in the humid climate region stabilizes the slope by reducing the infiltration of rain and binding loose soil particles with its root networks, serving as a natural retaining system. In that part of the study area, the landslide potential is high in forested areas, as intense rainstorms can lead to increased infiltration through dense vegetation, reducing soil shear strength and causing slope failure [32,36].

The density of vegetation is generally measured using the NDVI, which indicates that landslides, especially deep slides followed by debris flows, are prevalent in areas with a high NDVI value—areas covered by densely grown vegetation. In normal conditions, the vegetation cover prevents the formation of rain-triggered landslides. However, prolonged torrential rainfall allows for excessive infiltration in densely grown vegetation areas.

In the study area, small-scale landslides were frequently caused by the erosion of the natural slope due to the construction of roads and buildings. The erosion of steep gradient slopes leads to a higher risk of slope failure than that of gentle gradient slopes. Our results indicate that all the landslide types, except slump, are distributed within 20 m from a road where the slope gradient exceeds 30°. As slumps are largely formed in urban areas, determining whether or not the activities of road cuts induce the slump is challenging.

It is challenging to predict changes that might result from urbanization and to assess the potential for landslides in mountainous areas. However, it is common knowledge that urbanization often leads to alterations in the landscape and land cover. For example, the natural topography may be altered for construction purposes, and vegetation may be cleared for various reasons, such as wood harvesting, mining, and agriculture.

Our findings show that while overall landslide susceptibility increases with urbanization, certain landslide types show a decrease in occurrence due to changes in land cover. In Town Plans 1 and 2, deep-seated slides had a lower chance of occurring, as large-scale landslides that occurred in 2015 were rare in the urban area, except for a major soil slump that destroyed 473 buildings. It is important to note that the landslide model used in this analysis heavily relies on historical landslide information. According to the IVA, forest areas have a high potential for deep slides to occur. The results from our models indicate that urbanization, which involves the conversion of forests into built-up areas, reduces the likelihood of a deep slide occurring. Similarly, the potential for the occurrence of slumps decreased in Town Plan 1. The IVA also indicates that the slump potential is high in forest

and grassland areas. When these areas were converted to urban areas in Town Plan 1, the potential for slumps decreased in.

This research does, however, have certain limitations. The landslide model relies on historical landslide data, which in turn depends on the accuracy of the data inventory. Moreover, it is not possible to accurately predict landslides solely using remote sensing imagery, as small-scale landslides can be concealed by vegetation or landscape modifications after the failure. This can result in the underestimation of landslide susceptibility in areas characterized by mixed land-cover types, especially in urban areas. Furthermore, to accurately predict landslides before and after urban development, new layers were created from road networks and land-cover types. As a detailed road network plan could not be provided by government officials, the road network used in this study was determined using topographic features and traditional road construction methods. The road network design will likely change after the detailed design stage. Moreover, the future land-cover types of newly developed urban areas could not be accurately predicted; thus, the land-cover types of new towns were substituted and assigned weight on their thematic class, based on existing urban areas of Hakha City.

The accuracy of landslide susceptibility before and after urbanization was validated through observation of landslides in subsequent years. Two shallow landslides affected Town Plan 2 during the rainy season of 2016 when construction was underway. Hakha City, an existing urban area characterized by altered slopes, drainage systems, and sparse vegetation, has also experienced several small-scale landslides. However, there are no records of significant historical landslides.

#### 4. Conclusions

In 2015, Hakha City experienced landslides caused by heavy rainfall from Cyclone Komen, destroying over 1000 buildings and leaving their residents in need of resettlement. In this study, three proposed town plans for urban resettlement were evaluated in terms of their landslide risks and hazards to determine their degree of disaster risk in terms of landslide susceptibility. To assess landslide susceptibility of the town plans after urbanization, land-cover data from the city area were compared to land-cover data for each of the three town plans. A total of 112 landslides covering over an area of 3.63 km<sup>2</sup> were observed, and 4 types of landslides were identified. According to our IVA:

- Shallow slides were commonly observed as follows: on slopes between 20° and 50°, within 40 m from streams, at approximately a 50 m radius from natural springs, with a soil thickness of over 15 m, within urban and forest areas, and within 40 m from road cuts.
- Deep-seated slides were often induced by groundwater fluctuation and were abundantly observed as follows: in slope gradients of 30–40°, within 20 m from streams, within 100 m from natural springs, where colluvium soil more than 10 m deep is deposited, in forest areas, and within 40 m from road cuts.
- Slumps were commonly observed as follows: in slopes of less than 20°, within 100 m from natural springs, where colluvium soil of more than 10 m in depth is deposited, and in urban areas.
- Debris flows, caused by running water, were commonly observed as follows: within 20 m from streams, in forest lands or areas with dense vegetation, and within 40 m from an eroded slope.

Each of the four landslide types were formed under specific conditions, and the landslide susceptibility varied for each type. Based on the available data, the statistical modeling method was the most successful at predicting landslide susceptibility before and after urbanization. The analysis revealed that the hazard level increased to high and very high potential in Town Plans 1, 2, and 3 by 10%, 16%, and 5%, respectively. Town Plan 3 was found to be the most suitable with a low potential for landslides, followed by Town Plans 1 and 2. After urbanization, the potential for shallow slides and debris flows increased in all three plans.

The findings of this research show that urbanization poses an increased risk of landslides in the study area, although the impact is not significant. These findings can be used to predict the locations of high-risk areas and possible types of landslides and are expected to aid in the development of mitigation measures such as retaining walls, gabions, and drainage systems.

In conclusion, statistical modeling can be a highly effective approach to evaluating the susceptibility of landslides after urbanization. By using landslide inventories as dependent variables and the possible causes of landslides as independent parameters, it is possible to develop landslide susceptibility maps that incorporate changes in land cover and road networks due to urbanization. This study on landslide susceptibility in Hakha City revealed that the changes in landslide susceptibility before and after urbanization varied depending on the type of landslide. Although overall landslide susceptibility increased after urbanization, susceptibility for certain types of landslides decreased. In this study, an evidence-based statistical modeling approach was employed to analyze landslide susceptibility. This approach can be used during preliminary investigations of landslide risks in newly developed urban areas where proper infrastructure design and site investigation information may be lacking. By identifying susceptibility to specific types of landslides, we can develop more targeted risk reduction strategies that can help minimize the potential impact of landslides on urbanization.

**Author Contributions:** This research was conducted by the corresponding author K.S.M.T. for his requirement of partial fulfillment of a doctoral degree at the Asian Institute of Technology. The review and editing was conducted by the affiliated authors. All authors have read and agreed to the published version of the manuscript.

**Funding:** This research was funded by the Japan Government Scholarship and Asian Institute of Technology, and the Article Processing Charge (APC) was funded by the corresponding author.

**Institutional Review Board Statement:** This research is conducted by the requirement of fulfillment of doctoral degree of engineering in Asian Institute of Technology, and approved by board of examination committee. The approval number is not assigned by institute.

**Data Availability Statement:** The data in this research are from free-download satellite images and collected field data. The reference “Win M.; Kyaw H. Report on the Engineering Geology Aspects of Landslides and Road Subsidence in Hakha Township and Surrounding Areas, Chin State, Myanmar. Department of Geological Survey and Mineral Exploration (DGSME), Ministry of Mines, Republic of the Union of Myanmar, in collaboration with the Myanmar Geosciences Society (MGS). Personal communication, 2015” cannot be made available due to its status as an unpublished report.

**Acknowledgments:** The corresponding author would like to acknowledge his family, the Chin State Government, and the Hakha Community.

**Conflicts of Interest:** The authors declare no conflict of interest.

## References

1. Turner, A.K.; Schuster, R.L. *Landslides: Investigation and Mitigation. Special Report 247*; Transportation Research Board, National Academy Press: Washington, DC, USA, 1996; Volume 678, pp. 129–130.
2. Ozdemir, A.; Altural, T. A comparative study of frequency ratio, weights of evidence and logistic regression methods for landslide susceptibility mapping: Sultan Mountains, SW Turkey. *J. Asian. Earth Sci.* **2013**, *64*, 180–197. [[CrossRef](#)]
3. Xu, C.; Xu, X.; Dai, F.; Xiao, J.; Tan, X.; Yuan, R. Landslide hazard mapping using GIS and weight of evidence model in Qingshui river watershed of 2008 Wenchuan earthquake struck region. *J. Earth Sci.* **2012**, *23*, 97–120. [[CrossRef](#)]
4. Terlien, M.T.J.; van Westen, C.J.; van Asch, T.W.J. Deterministic modelling in GIS-based landslide hazard assessment. In *Advances in Natural and Technological Hazards Research*; Springer: Berlin/Heidelberg, Germany, 1995; Volume 5, pp. 57–77. [[CrossRef](#)]
5. Bender, F. Geology of Burma. In *Beiträge zur Regionalen Geologie der Erde, Band 16*; Bannert, D., Ed.; Gebrüder Borntraeger: Berlin, Germany, 1983; pp. 22–27.
6. The Global New Light of Myanmar. Cyclone Komen Weakens, Heavy Rain Continue across Myanmar. Available online: <https://reliefweb.int/report/myanmar/cyclone-komen-weakens-heavy-rainfall-continues-across-myanmar> (accessed on 14 November 2018).
7. UNICEF. *Chin Situation Report*; WASH Cluster Myanmar: Yangon, Myanmar, 2015.

8. Chin Committee for Emergency Response and Rehabilitation (CCERR). The Chin State Floods & Landslides: A Community-Led Response and Assessment. Available online: [http://themimu.info/sites/themimu.info/files/assessment\\_file\\_attachments/CCERRpublicationEng.pdf](http://themimu.info/sites/themimu.info/files/assessment_file_attachments/CCERRpublicationEng.pdf) (accessed on 14 November 2018).
9. National Natural Disaster Management Committee. Situation Report 2, Republic of the Union of Myanmar. 2015. Available online: <https://reliefweb.int/report/myanmar/situation-report-no2-national-natural-disaster-management-committee-17-august-2015> (accessed on 2 May 2016). (Unpublished Report).
10. Alaska Satellite Facility. About ALOS PALSAR. Available online: <https://www.asf.alaska.edu/sar-data/palsar/terrain-corrected-rtc/> (accessed on 26 January 2016).
11. Van Westen, C.; Alkema, D.; Damen, M.C.J.; Kerle, N.; Kingma, N.C. *Multi-hazard Risk Assessment: Distance Education Course Guidebook*; Version 2011; United Nation University–ITC School on Disaster Geo-information Management: Enschede, The Netherlands, 2011; pp. 3–67–3–74.
12. Win, M.; Kyaw, H. *Report on the Engineering Geology Aspects of Landslides and Road Subsidence in Hakha Township and Surrounding Areas, Chin State, Myanmar*. Department of Geological Survey and Mineral Exploration (DGSME), Ministry of Mines, Republic of the Union of Myanmar, in Collaboration with the Myanmar Geosciences Society; MGS: Naypyidaw, Myanmar, 2015; (Unpublished report).
13. USGS. Landsat Normalized Difference Vegetation Index. Available online: <https://www.usgs.gov/landsat-missions/landsat-normalized-difference-vegetation-index> (accessed on 18 April 2019).
14. Xu, D.; Guo, X. Compare NDVI extracted from Landsat 8 imagery with that from Landsat 7 imagery. *Am. J. Rem. Sens.* **2014**, *2*, 10–14. [[CrossRef](#)]
15. Ke, Y.; Im, J.; Lee, J.; Gong, H.; Ryu, Y. Characteristics of Landsat 8 OLI-derived NDVI by comparison with multiple satellite sensors and in-situ observations. *Remote Sens. Environ.* **2015**, *164*, 298–313. [[CrossRef](#)]
16. Yuan, F.; Wang, C.; Mitchell, M. Spatial patterns of land surface phenology relative to monthly climate variations: US Great Plains. *GIScience Remote Sens.* **2014**, *51*, 30–50. [[CrossRef](#)]
17. Yin, K.L. Statistical prediction model for slope instability of metamorphosed rocks. In *Proceedings of the 5th International Symposium on Landslides*; Bonnard, C., Ed.; Balkema: Rotterdam, The Netherlands, 1988; Volume 2, pp. 1269–1272.
18. Kanungo, D.P.; Arora, M.K.; Sarkar, S.; Gupta, R.P. Landslide Susceptibility Zonation (LSZ) Mapping—A Review. *J. South Asia Disaster Stud.* **2012**, *2*, 81–105.
19. Sarkar, S.; Kanungo, D.P.; Patra, A.K.; Kumar, P. GIS Based Landslide Susceptibility Mapping—A Case Study in Indian Himalaya. *Disaster Mitig. Debris Flows Slope Fail. Landslides* **2012**, 617–624.
20. Chen, W.; Li, W.; Hou, E.; Zhao, Z.; Deng, N.; Bai, H.; Wang, D. Landslide susceptibility mapping based on GIS and information value model for the Chencang District of Baoji, China. *Arab. J. Geosci.* **2014**, *7*, 4499–4511. [[CrossRef](#)]
21. Zhu, C.; Wang, X. Landslide susceptibility mapping: A comparison of information and weights-of-evidence methods in Three Gorges Area. In *2009 International Conference on Environmental Science and Information Application Technology*; IEEE: Piscataway, NJ, USA, 2009; Volume 3, pp. 342–346.
22. Ba, Q.; Chen, Y.; Deng, S.; Wu, Q.; Yang, J.; Zhang, J. An improved information value model based on gray clustering for landslide susceptibility mapping. *Int. J. Geo-Inf.* **2017**, *6*, 18. [[CrossRef](#)]
23. Corominas, J.; van Westen, C.; Frattini, P.; Cascini, L.; Malet, J.P.; Fotopoulou, S.; Catani, F.; Van Den Eeckhaut, M.; Mavrouli, O.; Agliardi, F.; et al. Recommendations for the quantitative analysis of landslide risk. *Bull. Eng. Geol. Environ.* **2014**, *73*, 209–263. [[CrossRef](#)]
24. TIBCO. Data Science Team User’s Guide. Available online: [https://docs.tibco.com/pub/sfire-dsc/6.5.0/doc/html/TIB\\_sfire-dsc\\_user-guide/GUID-07A78308-525A-406F-8221-9281F4E9D7CF.html](https://docs.tibco.com/pub/sfire-dsc/6.5.0/doc/html/TIB_sfire-dsc_user-guide/GUID-07A78308-525A-406F-8221-9281F4E9D7CF.html) (accessed on 16 December 2018).
25. Varnes, D.J. *Slope Movement Types and Processes: Special Report, 176*; Transportation Research Board, US National Research Council: New York, NY, USA, 1978; pp. 11–33.
26. Highland, L.; Bobrowsky, P.T. *The Landslide Handbook: A Guide to Understanding Landslides*; Geological Survey: Reston, VA, USA, 2008; pp. 10–30.
27. Australian Geomechanics Society. The Australian GeoGuides for Slope Management and Maintenance. *J. News Aust. Geomech. Soc.* **2007**, *42*, 168–169.
28. Fabbri, A.G.; Chung, C.F.; Napolitano, P.; Remondo, J.; Zêzere, J.L. Prediction rate functions of landslide susceptibility applied in the Iberian Peninsula. *WIT Trans. Model. Simul.* **2002**, *31*, 703–718.
29. Cruden, D.M.; Varnes, D.J. *Landslide Types and Processes, Special Report 247*; Transportation Research Board, National Academy of Sciences: New York, NY, USA, 1993; pp. 36–75.
30. Kim, M.S.; Onda, Y.; Uchida, T.; Kim, J.K. Effects of soil depth and subsurface flow along the subsurface topography on shallow landslide predictions at the site of a small granitic hillslope. *Geomorphology* **2016**, *271*, 40–54. [[CrossRef](#)]
31. Swanston, D.N.; Lienkaemper, G.W.; Mersereau, R.C.; Levno, A.B. Timber harvest and progressive deformation of slopes in southwestern Oregon. *Bull. Assoc. Eng. Geol.* **1988**, *25*, 71–381.
32. Forbes, K.; Broadhead, J.; Brardinoni, A.D.; Gray, D.; Stokes, B.V. Forests and landslides: The role of trees and forests in the prevention of landslides and rehabilitation of landslide-affected areas in Asia Second edition. *Rap. Publ.* **2013**, *2*, 1–61.
33. Hales, T.C. Modelling biome-scale root reinforcement and slope stability. *Earth Surf. Process. Landf.* **2018**, *43*, 2157–2166. [[CrossRef](#)]
34. Cohen, D.; Schwarz, M. Tree-root control of shallow landslides. *Earth Surf. Dyn.* **2017**, *5*, 451–477. [[CrossRef](#)]

35. Vergani, C.; Giadrossich, F.; Buckley, P.; Conedera, M.; Pividori, M.; Salbitano, F.; Rauch, H.S.; Lovreglio, R.; Schwarz, M. Root reinforcement dynamics of European coppice woodlands and their effect on shallow landslides: A review. *Earth-Sci. Rev.* **2017**, *167*, 88–102. [[CrossRef](#)]
36. Riechard, J.S. *Environmental Geology: Mass Wasting and Related Phenomena*; The McGraw Hill Companies: New York, NY, USA, 2011; pp. 194–221.

**Disclaimer/Publisher’s Note:** The statements, opinions and data contained in all publications are solely those of the individual author(s) and contributor(s) and not of MDPI and/or the editor(s). MDPI and/or the editor(s) disclaim responsibility for any injury to people or property resulting from any ideas, methods, instructions or products referred to in the content.